NJC

Accepted Manuscript

This is an *Accepted Manuscript*, which has been through the Royal Society of Chemistry peer review process and has been accepted for publication.

Accepted Manuscripts are published online shortly after acceptance, before technical editing, formatting and proof reading. Using this free service, authors can make their results available to the community, in citable form, before we publish the edited article. We will replace this *Accepted Manuscript* with the edited and formatted *Advance Article* as soon as it is available.

You can find more information about *Accepted Manuscripts* in the Information for Authors.

Please note that technical editing may introduce minor changes to the text and/or graphics, which may alter content. The journal's standard Terms & Conditions and the Ethical guidelines still apply. In no event shall the Royal Society of Chemistry be held responsible for any errors or omissions in this *Accepted Manuscript* or any consequences arising from the use of any information it contains.

ROYAL SOCIETY OF CHEMISTRY

www.rsc.org/njc

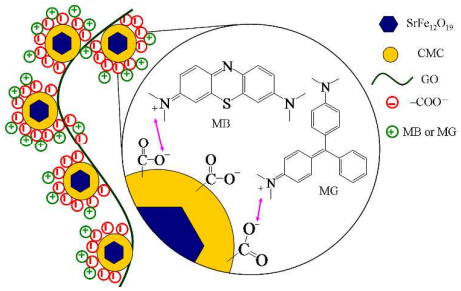

Magnetic adsorbents with more adsorption sites can realize an efficient adsorption of cationic dyes.

A novel magnetic polysaccharide/graphene oxide composite for removal of cationic dyes from aqueous solution

Liang Gao [a], Yaoguang Wang [a], Tao Yan [b], Limei Cui [b], Lihua Hu [a], Liangguo Yan [b], Qin Wei [a], Bin Du [a,*]

[a] Key Laboratory of Chemical Sensing & Analysis in Universities of Shandong, School of Chemistry and Chemical Engineering, University of Jinan, Jinan 250022, China

[b] School of Resources and Environment, University of Jinan, Jinan 250022, China

[*]Corresponding author. Tel: + 86 531 82767370; Fax: + 86 531 82767370.

E-mail address: dubin61@gmail.com (B. Du).

Abstract

In this paper, carboxymethyl functionalized chitosan was used for synthesis of magnetic polysaccharide/graphene oxide composite (SCGO). Compared with magnetic chitosan/graphene oxide composite reported before, adsorption capacity in this research had improved significantly. The calculated maximum adsorption capacity for methylene blue (MB) and malachite green (MG) were 358.4 mg/g and 289.1 mg/g, respectively. The morphology, chemical properties and physical structure of the SCGO were characterized by scanning electron microscopy (SEM), Fourier transform infrared spectroscopy (FTIR) and X-ray powder diffraction (XRD). The influence factors which included pH, adsorbent dose, ionic strength and contact time on the adsorption properties of MB and MG onto SCGO were investigated. The adsorption kinetics of MB and MG on SCGO were well-described by pseudo-second order kinetic models. The experimental data of isotherm followed the Temkin isotherm model and the Langmuir model, respectively. Thermodynamic analysis was also performed to calculate the changes in free energy (ΔG), enthalpy (ΔH), and entropy (ΔS). The results obtained from this research suggested that SCGO was a potential adsorbent for effective removal of methylene blue and malachite green.

Keywords: Carboxymethyl chitosan, Graphene oxide, Cationic dye, Magnetic adsorbent

1. Introduction

In recent years, environmental problems have become a global concern because of their impacts on human health. Nearly a quarter of the diseases that humans are

facing today are due to long-term exposure to environmental pollution which includes air, soil, and water pollution [1]. The increasing attention to public health and environmental quality has aroused special interest in developing and implementing various methods of removing potentially toxic organic and inorganic pollutants from water [2]. Dyeing effluent is one of the largest contributors to water contamination which has a destructive impact on environment security and human health [3]. Particularly, the cationic dye, such as methylene blue (MB) and malachite green (MG), can produce a series of grievous environmental problems.

MB is a kind of cationic pollutant which is quite difficult to be degraded in natural environment. It has wide applications in many fields [4]. It can induce eye burns in humans and animals, methemoglobinemia, cyanosis, convulsions, tachycardia, dyspnea, irritation to the skin, and if ingested, irritation to the gastrointestinal tract, nausea, vomiting, and diarrhea [5]. MG is a synthetic tri-phenyl methane dye. It has been widely used for dyeing as well as a fungicide and ectoparasiticide in aquaculture and fisheries [6]. MG has aroused much concern. Not only does the dye affect the chrominance of stream, but also it is carcinogenic and mutagenic [7, 8].

Therefore, there is considerable need to treat these dye effluents prior to their discharge into receiving waters. To prevent dyes contamination, various methods have been developed to remove dyes from aqueous environment, such as advance oxidation [9], photocatalysis [10], adsorption [11], membrane filtration [12], and coagulation [13]. Among these methods, the adsorption technique is especially attractive because of its high efficiency, simplicity of design, and ease of operation [14].

In the past researches, activated carbon had caused wide public concern, but its high cost poses an economical problem. In recent years, many researches have focused on the use of various cheaper adsorbents instead of activated carbon. The new trends are focused on carbon- and polysaccharide-based materials [15].

Graphene, a novel one-atom-thick two-dimensional graphitic carbon system, is a star in materials science and condensed-matter physics [16]. In recent years, researchers have developed a series of methods to prepare graphene, such as sonication induced exfoliation [17], laser induced exfoliation [18, 19], unzipping of carbon nanotubes either by laser [20] or by chemical treatment [21], and laser reduction of graphene oxide [22, 23]. Graphene oxide (GO) has a layered structure similar to graphene, but the plane of carbon atoms in GO is decorated by oxygen-containing groups. GO has multiple oxygen-containing functional groups (carboxyl, hydroxyl and epoxy) that attached to its layers covalently, resulting in a negatively charged surface. It was studied as a potential adsorbent, and its ability to remove cationic dyes has been demonstrated [24, 25].

Chitosan is a multifunctional polymer that has hydroxyl groups and highly reactive amino groups. It is used in food, cosmetics, biomedical and pharmaceutical applications, etc [26]. Numerous investigations on the chemical activation of chitosan have been carried out to increase its adsorption capacity for dyes [27]. However, the hydrophilic property of chitosan should be improved for practical operation. In order to improve the hydrophilic property and further enhance the adsorption capacity for dye, chemical modification is required. Carboxymethyl chitosan (CMC) is an

amphiprotic chitosan derivative, which contains hydroxyl (–OH), carboxyl (–COOH) and amine ($–NH_2$) groups in the molecule, and makes it possible to improve the hydrophilic property of CMC and provide enough adsorption groups for increasing adsorption capacity toward dyes [28].

The conventional absorbents have a major drawback that absorbents are difficult to separate from the liquid. Magnetic separation technique has been shown to be a promising method for solid-liquid phase separation. It was convenient to separate the magnetic absorbents from aqueous solution in an external magnetic field [29, 30]. Strontium ferrite is a typical hard magnetic material with the hexagonal magnetoplumbite type. It is not easy to be demagnetized after magnetized and has been widely used in the industrial field.

Magnetic chitosan and magnetic graphene oxide have been widely used in drug delivery [31, 32], cell separation [33], enzyme immobilization [34], catalysis [35, 36], and removal of pollutants [37, 38]. Magnetic chitosan grafted with graphene oxide have been reported remove dyes [15, 39, 40]. However the adsorption capacity of these adsorbents was much lower than expectation. The reason might be that the cross-linking agent occupied effective adsorption sites. In the past researches, excessive glutaraldehyde was used as the cross-linking agent to link amino groups that were the active sites of adsorption and, hence, the adsorption capacity was greatly reduced. In this work, chitosan was replaced with CMC, about eighty percent of amino groups in which were superseded by carboxymethyl. The use of CMC not only offered linking groups ($–NH_2$), but also reserved sufficient active sites (–COOH). The deprotonated carboxyl groups could

catch the cationic dyes by electrostatic interactions (Schematic 1). Adsorption performance of adsorbents was improved obviously. As-prepared strontium ferrite-CMC-GO compound (SCGO) was used to remove MB and MG and displayed excellent separation property and adsorption capacity. Furthermore, the kinetic and isotherm studies on MB and MG adsorption by SCGO were also investigated in this study.

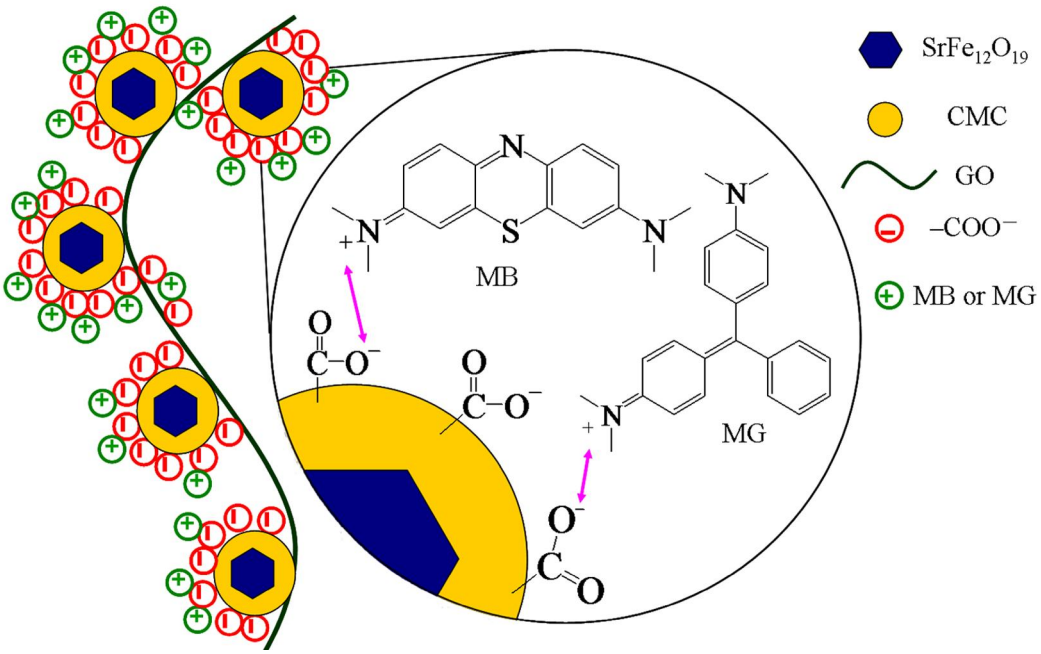

Schematic 1 Proposed mechanism of MB and MG Adsorption onto SCGO.

2. Material and methods

2.1 Materials

Nano strontium ferrite owning an average size of about 80 nm was purchased from Nanjing Emperor Nano Material Co., Ltd. and carboxymethyl chitosan was obtained from Nantong Lvshen Biological Engineering Co., Ltd., whose substitution degree was not lower than eighty percent. Other chemicals, obtained from Sinopharm Chemical Reagent Beijing Co. Ltd., China, are of analytical reagent grade. Ultrapure

126 water (EASY-pure LF, Barnstead International, Dubuque, IA, USA) was used
127 throughout the experiment.

128 *2.2 Preparation of adsorbent*

129 *2.2.1 Preparation of GO*

130 The GO were synthesized on the basis of the improved method reported by
131 Daniela C. Marcano et al [41]. For the improved method, a 9:1 mixture of concentrated
132 H_2SO_4/H_3PO_4 (72:8 mL) was added to a mixture of graphite powder (0.6 g) and
133 $KMnO_4$ (3.6 g). The reaction system was heated to 50 ºC and stirred for 12 h. Then
134 the reaction was cooled to room temperature and poured onto ice (about 80 mL) with
135 30% H_2O_2 (1 mL). The product was centrifuged, and the supernatant was decanted
136 away. Next the remaining solid material was washed three times with HCl (0.2 mol/L)
137 and ethanol, respectively. Afterwards it was washed with ether. Finally the obtained
138 solid was dried in vacuum at 35 ºC.

139 *2.2.2 Preparation of SCGO*

140 The preparation process of SCGO was as follows: 0.3 g of pure carboxymethyl
141 chitosan was dissolved in 30 mL ultrapure water, and the mixture was sonicated at
142 room temperature for 3 h. Then, 0.1 g of magnetic nanosized strontium ferrite was
143 added to the colloidal solution and the reaction system was continually stirred using
144 electric blender for 1.5 h. Subsequently, 3 mL liquid paraffin was dispersed slowly in
145 the mixture under stirring. After 0.5 h of emulsification, 3 mL of glutaraldehyde was
146 added dropwise as cross-linker. Next, 0.2 g of GO was added to the reaction flask, and
147 the mixed system was stirred continuously for 1.5 h in an oil bath at 50 ºC. After that

148 the mixture was adjusted to pH 9-10 using sodium hydroxide solution, and kept in an
149 oil bath for another 1 h at 80 ºC. The product was washed with petroleum ether,
150 ethanol and ultrapure water in turn. Then, the precipitate was dried in vacuum. The
151 final product (SCGO) was ground to a fine powder.

152 *2.3 Characterization methods*

153 The morphology observation of SCGO was carried out by using a QUANTA
154 FEG 250 scanning electron microscopy (FEI, United States). FTIR spectra of the
155 samples were obtained from a Perkin-Elmer Spectrum One FTIR spectrometer
156 (Perkin–Elmer, United States). The spectra were recorded from 4000 to 400 cm^{-1}.
157 X-ray powder diffraction (XRD) patterns were recorded on a D8 FOCUS X-ray
158 diffraction spectrometer (Bruker, Germany) with Cu Kα radiation for crystalline phase
159 identification. The sample was scanned from 5º to 80º.

160 *2.4 Batch adsorption experiments*

161 The batch adsorption experiments were carried out to determine the adsorption
162 capacity for two dyes on SCGO. In a typical batch adsorption experiment procedure,
163 different quantities of adsorbent (3-13 mg) were agitated with 25 mL of a solution
164 containing 140 mg/L MB or 70 mg/L MG in 100 mL air-tight conical flask for 3 h.
165 The effect of pH on the adsorption of SCGO composites for MB and MG was
166 evaluated in the pH range of 1-10 for MB and 2-8 for MG respectively. The initial pH
167 values of solutions were adjusted using NaOH and HCl. The salt concentration was
168 adjusted for 0 to 0.10 mol/L using NaCl to investigate the effect of ionic strength.
169 Adsorption kinetics was carried out at 308 K and predetermined pH for different time.

The batch experiments for adsorption studies were also carried out at different temperatures (298K, 308K and 318K) with different initial concentration of MB (20-200 mg/L) or MG (10-150 mg/L). The solid phase was separated from the solution using a magnet. The equilibrium concentrations of dyes were determined at the best coloration pH of dyes using a UV-vis spectrophotometer.

The removal efficiency and the adsorption amount q_t (mg/g) were calculated based on the difference of the MB or MG concentration in the aqueous solution before and after adsorption according to the formula:

$$\text{Removal efficiency (\%)} = (c_o - c_t)/c_o \times 100\% \quad (1)$$

$$q_t = (c_o - c_t) \times V / m \quad (2)$$

Where c_t (mg/L) is the concentration of adsorbate at time t (min), V (L) is the volume of adsorbate solution, m (g) is the mass of adsorbents, q_t (mg/g) is the adsorbed amount at time t (min).

3. Results and discussion

A novel magnetic polysaccharide/graphene oxide composite (SCGO) had been prepared, and was characterized by SEM, FTIR and XRD. The adsorption of MB and MG onto SCGO was investigated to confirm the optimal adsorption conditions and possible adsorption mechanism by batch adsorption experiments.

3.1 Characterization of adsorbent

The morphology of SCGO was investigated by scanning electron microscopy (SEM). Fig. 1A shows a typical SEM image of GO, which presents a sheetlike structure with large thickness, smooth surface, and wrinkled edge. After the

combination with nano strontium ferrite coated CMC to form the SCGO composite (Fig. 1B), the SCGO exhibited a much rougher surface, revealing that nano strontium ferrite coated CMC has been assembled on the surface of GO layers.

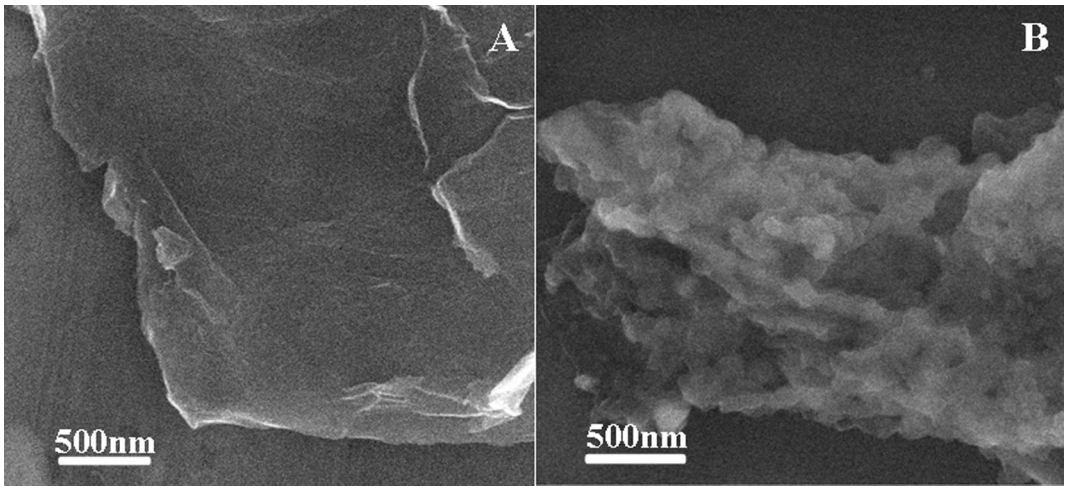

Fig. 1 SEM images of GO (A) and SCGO (B).

The FTIR spectra of SCGO, which was shown in Fig. 2A, revealed the presence of the oxygen-containing functional groups. The broad absorption band at 3444 cm^{-1} was attributed to O–H stretching vibration. The peak at 2923 cm^{-1} corresponded to saturated C–H of carboxymethyl chitosan. The characteristic absorbance band at 1616 cm^{-1} and the peak at 1398 cm^{-1} were due to the presence of –COOH. The peak at 1121 cm^{-1} was attributed to C–O–C stretching vibration and the peak at 601 cm^{-1} corresponded to strontium ferrite.

XRD pattern of SCGO was shown in Fig. 2B. The positions and relative intensities of all diffraction peaks matched well with those from the Jade PDF card (shown in the top half of Fig. 2B) for strontium ferrite, indicating the existence of strontium ferrite.

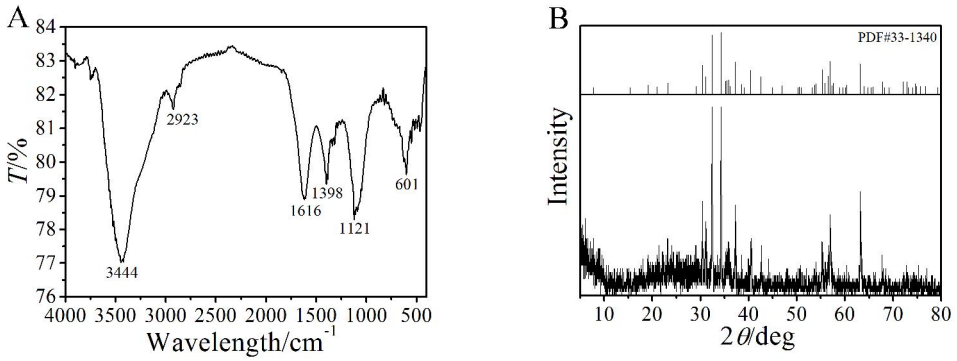

Fig. 2 FTIR spectra (A) and XRD pattern (B) of SCGO.

3.2 Effect of initial pH value on adsorption

The effect of pH is an important parameter of the general so-called adsorption process, which affects the adsorption of a pollutant. The effect of pH on the adsorption capacity of dyes was investigated in this study. Batch equilibrium adsorption experiments of MB and MG onto SCGO were carried out with a fixed 25 mL, 140 mg/L MB solution or 70 mg/L MG solution for long enough at room temperature. The pH was controlled with HCl and NaOH. As shown in Fig. 3, it could be clearly observed that there was a significant change on the adsorption capacities of MB and MG with pH increasing. The removal efficiencies of the two kinds of dyes were low at pH < 4, while pH > 4, the removal of MB and MG increased and the largest removal were over 90%.

The pH of dye solutions plays an important role in the adsorption process and particularly in adsorption capacity in the following three points: Firstly, the type and magnitude of charge on the dye species predominating in solution will determine whether the removal will take place or not. Secondly, the magnitude of the charge of the dye will determine the molar ratio adsorbent/dye suitable for maximum removal of dye. Thirdly, the mature of the dye predominant in the solution determines the state

of the collector/dye. Therefore, it determines the mechanism of the adsorbent separation [42].

The mechanisms of the adsorption process of cationic dyes on the SCGO were due to the ionic interactions of the dyes with the carboxyl groups of the SCGO. In aqueous solution, the cationic dyes were first dissolved and converted to cationic dye ions.

The carboxyl groups of SCGO were deprotonated under relatively alkaline conditions (pH > 4) according to the following reaction:

$$\text{R-COOH} \leftrightarrow \text{R-COO}^- + \text{H}^+$$

$$\text{R-COOH} + \text{OH}^- \leftrightarrow \text{R-COO}^- + \text{H}_2\text{O}$$

The adsorption process then proceeded due to the electrostatic attraction between these two oppositely charged ions.

$$\text{R-COO}^- + \text{Dye}^+ \leftrightarrow \text{R-COO}^- \cdots \text{Dye}^+$$

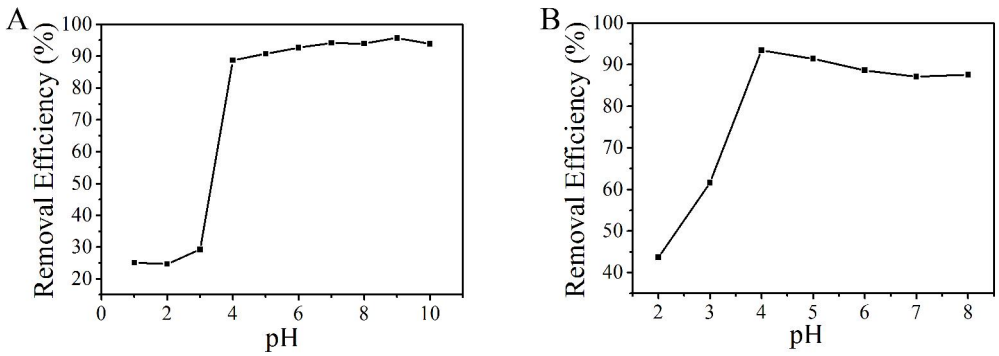

Fig. 3 Effect of pH on adsorption of MB (A) and MG (B) onto SCGO.

3.3 Effect of adsorbent dose

The effect of the adsorbent dose was investigated by addition of various amounts of SCGO in 25 mL aqueous solution (140 mg/L and 70 mg/L for MB and MG, respectively) at room temperature for 3 h.

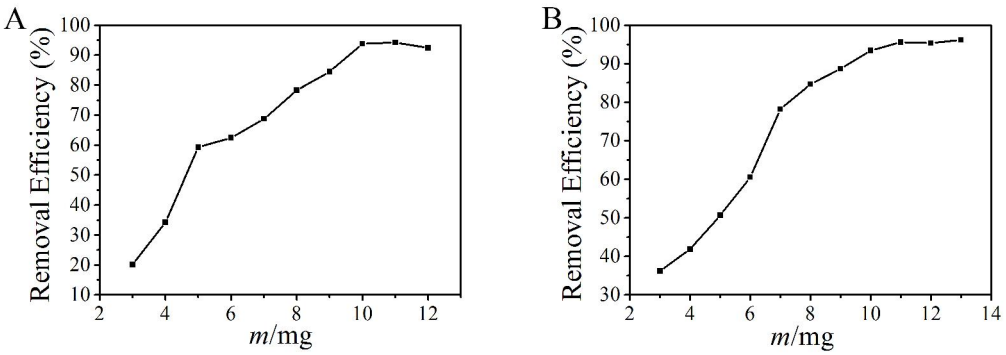

Fig. 4 Effect of adsorbent dose on the adsorption of MB (A) and MG (B) onto SCGO.

As shown in Fig. 4, it was observed that the adsorption efficiency of the two dyes increased with increasing initial amount of adsorbent and reached to a plateau at 10 mg for MB and 11 mg for MG, respectively.

3.4 Effect of ionic strength

The effect of ionic strength on the adsorption of MB and MG onto SCGO was studied under different NaCl concentration (Fig. 5). It could be seen that the removal efficiency decreased with increasing NaCl concentration. The adsorption percentages of dyes on SCGO decreased by more than 20% as the concentration of NaCl in solution increased from 0 to 0.10 mol/L. The ionic strength played a key role in controlling electrostatic interactions. Hence, these interactions, attractive or repulsive, were decreased with increasing NaCl concentration. High ionic strength would cause a screening effect [43]. The increase in ionic strength would inhibit the electrostatic interactions between the cationic dyes and the deprotonated carboxyl groups of SCGO[44]. Moreover, high ionic strength also could decrease the electrostatic repulsion between SCGO, which results in aggregation and lower adsorption ability of SCGO [45].

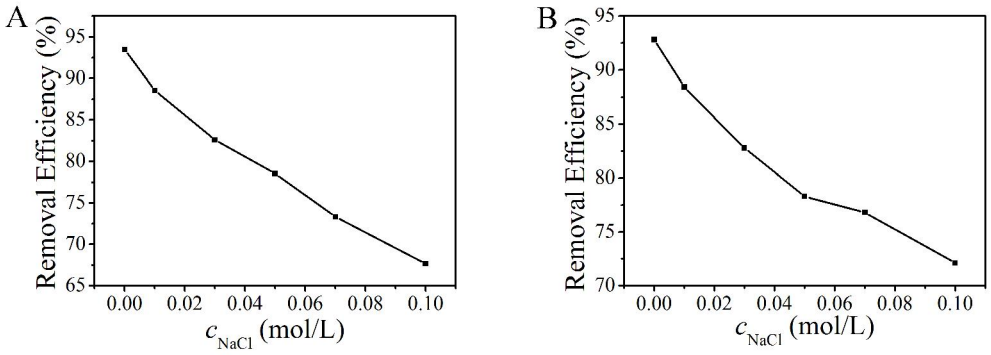

Fig. 5 Effect of ionic strength on the adsorption of MB (A) and MG (B) onto SCGO.

3.5 Adsorption kinetics

Kinetics of the adsorption process is vital in wastewater treatment, as it provides essential information on the solute uptake rate and the reaction pathways. The effect of contact time on dyes adsorption by SCGO was illustrated in Fig. 6. It showed that the removal efficiency of the two dyes reached equilibrium at 20 min for MB and 60 min for MG.

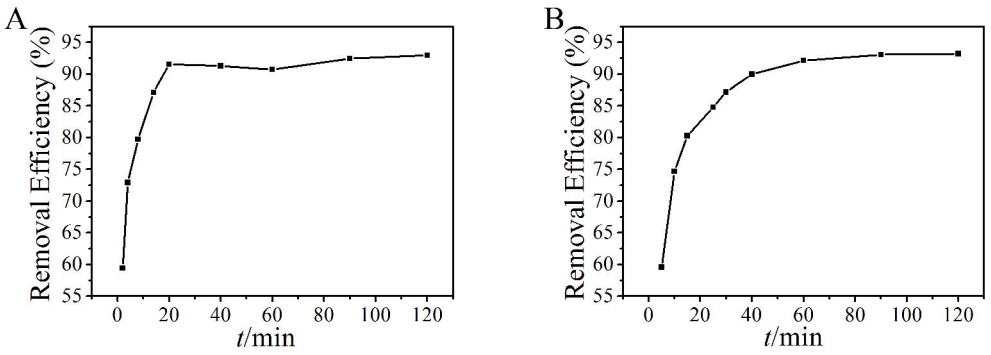

Fig. 6 Effects of contact time on adsorption of MB (A) and MG (B) onto SCGO.

The adsorption kinetics data of heavy metal ions were analyzed by testing pseudo-first order kinetic model and pseudo-second order kinetic model [46], which can be expressed as follows:

Pseudo-first-order kinetics:

$$\ln(q_e - q_t) = \ln q_e - k_1 t \quad (3)$$

279 Pseudo-second-order kinetics:

280 $$\frac{t}{q_t} = \frac{1}{k_2 q_e^2} + \frac{t}{q_e} \quad (4)$$

281 Where q_t (mg/g) and q_e (mg/g) are the adsorption capacities at time t (min) and
282 equilibrium, respectively, k_1 (min^{-1}) and k_2 (g/(mg min)) are the pseudo-first-order
283 and pseudo-second-order rate constant.

284 The fitted curves are shown in Fig. 7, and the parameters were calculated and
285 listed in Table 1. From the fitting result, it was found that the measured kinetic data of
286 MB and MG adsorbed by SCGO fitted pseudo-second order kinetic model with a
287 correlation coefficient of 0.9989 and 0.9998, respectively. Moreover, the experimental
288 equilibrium adsorption capacity of MB and MG (320.3 mg/g and 148.0 mg/g) fit well
289 with the calculated value (330.0 mg/g and 154.1 mg/g) of pseudo-second-order kinetic
290 model.

291 Table 1 Constants and correlation coefficients for the kinetic models.

Model	Parameter	MB	MG
Pseudo-first-order kinetic model	q_e (mg/g)	123.4	58.65
	k_1 (min^{-1})	0.1434	0.06036
	R^2	0.9312	0.9871
Pseudo-second-order kinetic model	q_e (mg/g)	330.0	154.1
	k_2 (g/(mg min))	0.002475	0.002003
	R^2	0.9989	0.9998

292

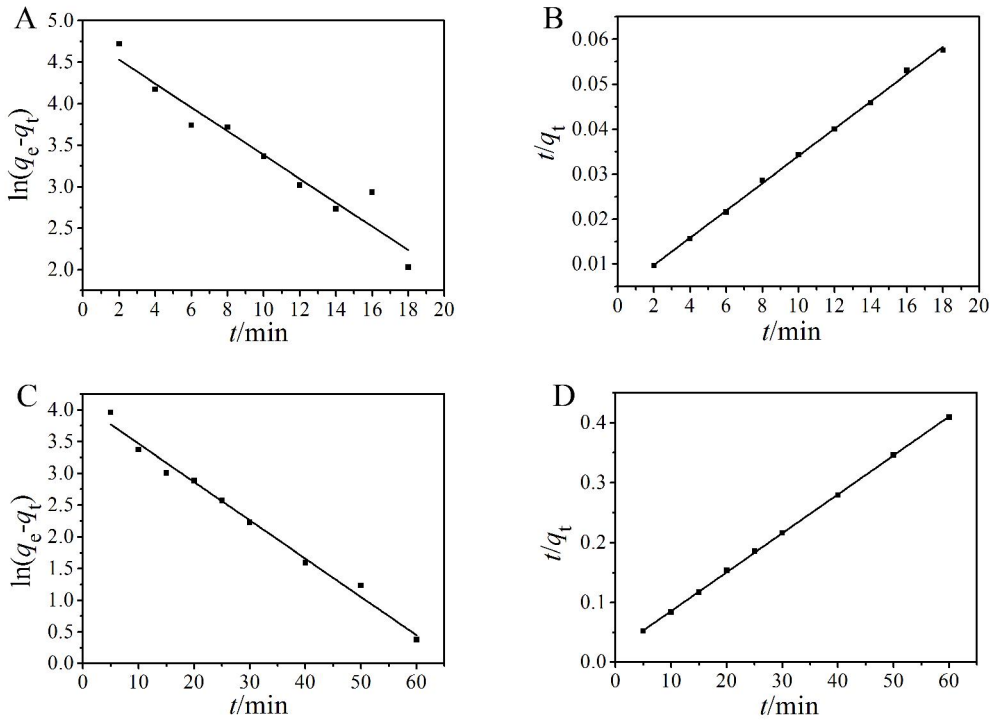

Fig. 7 Pseudo-first-order kinetics (A), pseudo-second-order kinetics (B) fit of MB and pseudo-first-order kinetics (C), pseudo-second-order kinetics (D) fit of MG adsorption on SCGO.

3.6 Adsorption isotherm

The adsorption isotherms of SCGO for MB and MG were investigated under the optimized conditions obtained before over a wide range of initial concentration of MB (20-200 mg/L) and MG (10-150 mg/L) at 308K. Four isotherm equations were selected for the study of modeling these adsorption isotherm data: Henry [47], Langmuir [48], Freundlich [48], and Temkin [49] equations, expressed as follows:

Henry model:

$$q_e = kc_e \quad (5)$$

Langmuir model:

$$q_e = \frac{bq_m c_e}{1+bc_e}, \quad \frac{1}{q_e} = \frac{1}{bq_m}\cdot\frac{1}{c}+\frac{1}{q_m} \quad (6)$$

Freundlich model:

$$q_e = K_F c_e^{1/n},\ \ln q_e = \ln K_F + \frac{1}{n}\ln c_e \quad (7)$$

Temkin model:

$$q_e = \frac{RT}{b_T}\ln c_e + \frac{RT}{b_T}\ln A_T \quad (8)$$

The fitting results getting from the isotherms are shown in Fig. 8 and Fig. 9, and the values of correlation coefficients and other parameters obtained from the adsorbent are given in Table 2.

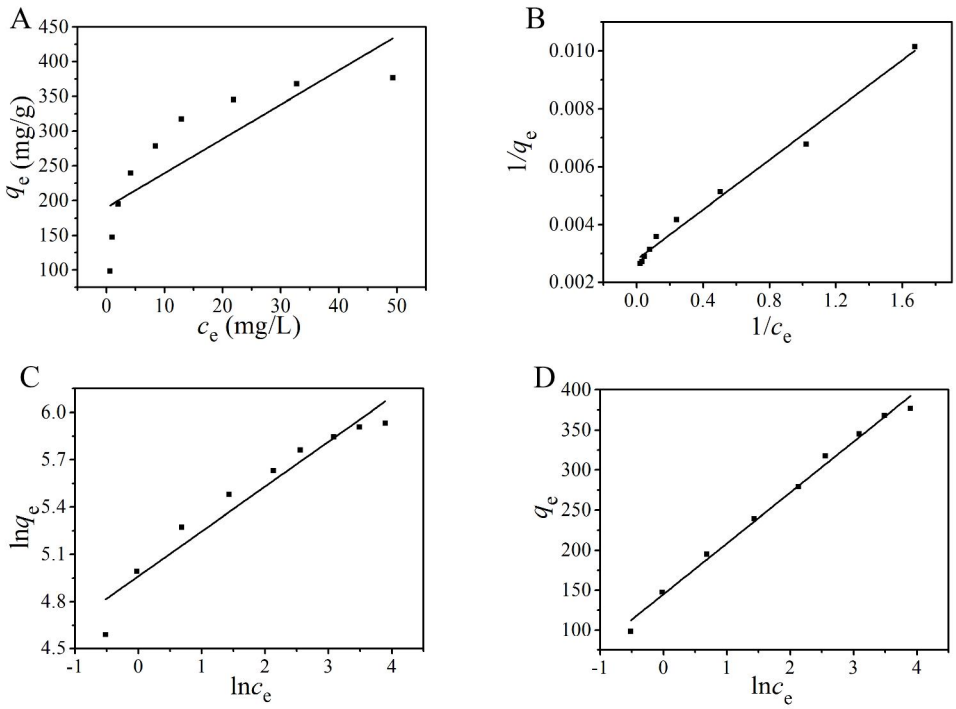

Fig. 8 Henry (A), Langmuir (B), Freundlich (C), and Temkin (D) adsorption isotherm fit of MB adsorption onto SCGO.

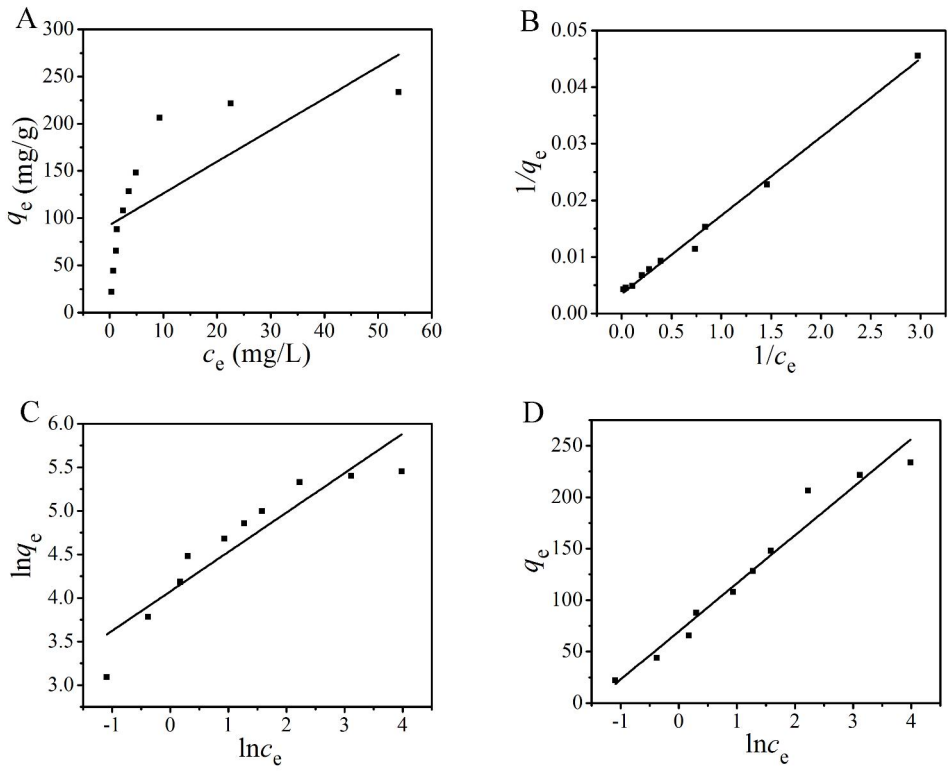

Fig. 9 Henry (A), Langmuir (B), Freundlich (C), and Temkin (D) adsorption isotherm fit of MG adsorption onto SCGO.

As shown in Table 2, it is found that the Langmuir model was suitable for describing the adsorption of MB and MG on SCGO (R^2 >0.98), which implied that the adsorption of molecule is a monolayer adsorption and the adsorption of adsorbent surface is uniform.

While it should be noted that Temkin model was more suitable than Langmuir model for the adsorption of MB on SCGO. This result might ascribe that the concentration of MB was so high that interaction among adsorbed molecules could not be ignored absolutely. The adsorption process diverged from Langmuir model to Temkin model.

The data of maximum adsorption capacity for the adsorption of MB or MG onto various magnetic adsorbents were shown in Table 3. It could be obtained that SCGO

possessed higher adsorption capacity than that of many magnetic adsorbents reported before.

Table 2 Constants and correlation coefficients of adsorption isotherms for the adsorption.

Model	Parameter	MB	MG
Henry equation	k	4.941	3.351
	R^2	0.6538	0.580
Langmuir equation	q_m (mg/g)	358.4	289.1
	b (L/mg)	0.6473	0.2496
	R^2	0.9879	0.9939
Freundlich equation	K_F	142.9	58.84
	n	3.518	2.209
	R^2	0.9267	0.8522
Temkin equation	b_T	40.35	54.81
	A_T	9.843	4.448
	R^2	0.9908	0.9582

Table 3 Maximum adsorption capacity for the adsorption of MB or MG onto various magnetic adsorbents.

Adsorbent	Adsorbate	Adsorption capacity (mg/g)	Reference
GNS/Fe_3O_4	MB	43.82	[16]
MCGO	MB	180.83	[39]
GO–Fe_3O_4	MB	167.2	[50]
OC-BzM	MB	223.58	[51]
Fe_3O_4@HHSS	MB	71.45	[52]
GO-CA-Fe_3O_4	MB	112	[53]
SCGO	MB	358.4	This work
OC-BzM	MG	144.79	[51]
AC/CFO	MG	89.29	[54]
MRGO	MG	22	[55]
Alg–Fe_3O_4	MG	47.84	[56]
Fe_3O_4/MWCNT	MG	55.25	[57]
SCGO	MG	289.1	This work

3.7 Adsorption thermodynamics

The investigation of temperature effect on dye molecules adsorption onto collector was carried out at temperatures ranging from 298 to 318 K. The change in ΔG was calculated with Eq. (9). ΔH and ΔS were calculated from the slope and intercept of the plot of $\ln K_d$ versus $1/T$ using Eq. (10).

$$\Delta G = -RT \ln K_d \quad (9)$$

$$\ln K_d = \frac{\Delta S}{R} - \frac{\Delta H}{RT} \quad (10)$$

Where ΔG (kJ/mol) is the Gibbs free energy change of sorption, ΔH (kJ/mol) is the enthalpy change, ΔS (J/mol K) is the entropy change, T (K) is the temperature in Kelvin, R (8.314 J/mol K) is universal gas constant and K_d (L/g) is the thermodynamic equilibrium constant that were computed by plotting $\ln(q_e/c_e)$ versus q_e and extrapolating q_e to zero [58].

The linear plot of $\ln K_d$ versus $1/T$ and thermodynamic parameters were listed in Fig. 10 and Table 4. The negative value of ΔG and positive value of ΔH indicated that the adsorption of MB and MG onto SCGO is a spontaneous and endothermic process. It revealed that the endothermic adsorption of MB and MG onto SCGO was enhanced by an increase in temperature. The positive value of ΔS stated clearly that the randomness increased at the solid–solution interface during the MB and MG adsorption. During adsorption, the coordinated water molecules, which were displaced by the dye molecules, gained more translational entropy than the lost by dye molecules, resulting in increased randomness in the dye−adsorbent interaction [59].

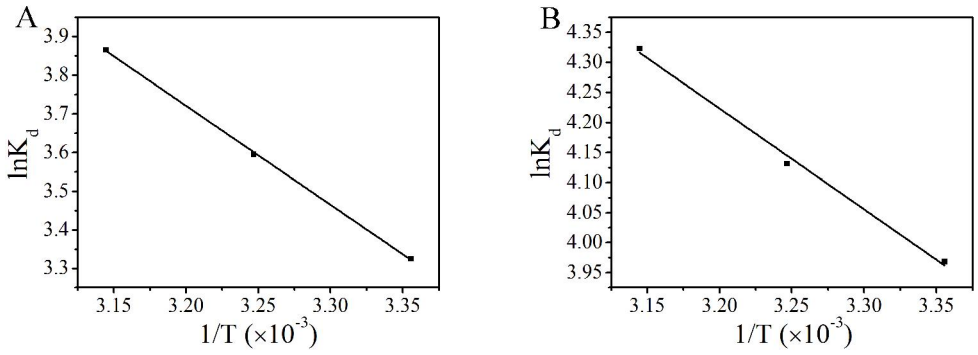

Fig. 10 Adsorption thermodynamics of MB (A) and MG (B) onto SCGO

Table 4 Thermodynamic parameters of the adsorption of MB and MG by SCGO.

Dye	T (K)	ΔG (kJ/mol)	ΔH (kJ/mol)	ΔS (J/mol K)
MB	298	– 8.24	21.30	99.09
	308	– 9.21		
	318	– 10.38		
MG	298	– 9.62	13.95	79.74
	308	– 10.35		
	318	– 11.18		

4. Conclusions

This study improved magnetic chitosan grafted with graphene oxide. Carboxymethyl chitosan replaced general chitosan to provide more active adsorption sites. The adsorption capacity of the novel adsorbent increased obviously than the previous researches. Batch adsorption experiments were carried out under various conditions, such as adsorbent dose, pH, ionic strength and contact time. The adsorption kinetics, adsorption isotherms and adsorption thermodynamics of magnetic polysaccharide/graphene oxide composite for methylene blue and malachite green were investigated. The results showed that the adsorption kinetics could be modeled by the pseudo second-order rate equation, and the process could reach equilibrium soon. The adsorption of methylene blue and malachite green on magnetic polysaccharide/graphene oxide composite conformed to Temkin model and Langmuir model respectively. Both isotherm and kinetic results revealed a chemical process for removal of methylene blue and malachite green. The adsorption was a spontaneous

and endothermic process. The results suggested that the magnetic polysaccharide/graphene oxide composite could be considered as a good alternative for extracting the dye from aqueous media.

Acknowledgments

This study was supported by the Natural Science Foundation of China (No. 21175057, 21377046), the Science and Technology Plan Project of Jinan (No. 201307010), the Science and Technology Development Plan of Shandong Province (No. 2014GSF120004), the Special Project for Independent Innovation and Achievements Transformation of Shandong Province (2014ZZCX05101).

References

1. L. Zhou, C. Gao and W. Xu, *ACS Appl. Mater. Inter.*, 2010, **2**, 1483-1491.
2. A. N. Chowdhury, S. Jesmeen and M. Hossain, *Polym. Adv. Technol.*, 2004, **15**, 633-638.
3. R. S. Blackburn, *Environ. Sci. Technol.*, 2004, **38**, 4905-4909.
4. Y. Yao, F. Xu, M. Chen, Z. Xu and Z. Zhu, *Bioresour. Technol.*, 2010, **101**, 3040-3046.
5. S. Senthilkumaar, P. Varadarajan, K. Porkodi and C. Subbhuraam, *J. Colloid. Interface. Sci.*, 2005, **284**, 78-82.
6. S. Srivastava, R. Sinha and D. Roy, *Aquat. Toxicol.*, 2004, **66**, 319-329.
7. O. Hernandez-Ramirez and S. M. Holmes, *J. Mater. Chem.*, 2008, **18**, 2751-2761.
8. G. Crini, *Bioresour. Technol.*, 2006, **97**, 1061-1085.

9. B. Shi, G. Li, D. Wang, C. Feng and H. Tang, *J. Hazard. Mater.*, 2007, **143**, 567-574.

10. G. Chen, M. Sun, Q. Wei, Y. Zhang, B. Zhu and B. Du, *J. Hazard. Mater.*, 2013, **244**, 86-93.

11. X. Guo, Q. Wei, B. Du, Y. Zhang, X. Xin, L. Yan and H. Yu, *Appl. Surf. Sci.*, 2013, **284**, 862-869.

12. C.-H. Lin, C.-H. Gung, J.-J. Sun and S.-Y. Suen, *J. Membrane Sci.*, 2014, **471**, 285-298.

13. W. Chen, W. Lu, Y. Yao and M. Xu, *Environ. Sci. Technol.*, 2007, **41**, 6240-6245.

14. Y. Wong, Y. Szeto, W. Cheung and G. McKay, *Langmuir*, 2003, **19**, 7888-7894.

15. N. A. Travlou, G. Z. Kyzas, N. K. Lazaridis and E. A. Deliyanni, *Langmuir*, 2013, **29**, 1657-1668.

16. L. Ai, C. Zhang and Z. Chen, *J. Hazard. Mater.*, 2011, **192**, 1515-1524.

17. Y. Hernandez, V. Nicolosi, M. Lotya, F. M. Blighe, Z. Sun, S. De, I. McGovern, B. Holland, M. Byrne and Y. K. Gun'Ko, *Nat. nanotechnol.*, 2008, **3**, 563-568.

18. P. Kumar, *RSC Adv.*, 2013, **3**, 11987-12002.

19. U. Maitra, H. Matte, P. Kumar and C. Rao, *Chimia*, 2012, **66**, 941-948.

20. P. Kumar, L. Panchakarla and C. Rao, *Nanoscale*, 2011, **3**, 2127-2129.

21. D. V. Kosynkin, A. L. Higginbotham, A. Sinitskii, J. R. Lomeda, A. Dimiev, B.

426 K. Price and J. M. Tour, *Nature*, 2009, **458**, 872-876.

427 22. P. Kumar, K. Subrahmanyam and C. Rao, *Int. J. Nanosci.*, 2011, **10**, 559-566.

428 23. P. Kumar, B. Das, B. Chitara, K. Subrahmanyam, K. Gopalakrishnan, S.

429 Krupanidhi and C. Rao, *Macromol. Chem. Phys.*, 2012, **213**, 1146-1163.

430 24. W. Ya-Ling, G. Peng, H. Lang-Huan, W. Xiao-Jing and L. Ying-Liang, *Chinese*

431 *J. Inorg. Chem.*, 2012, **28**, 391-397.

432 25. S.-T. Yang, S. Chen, Y. Chang, A. Cao, Y. Liu and H. Wang, *J. Colloid.*

433 *Interface. Sci.*, 2011, **359**, 24-29.

434 26. M. Rinaudo, *Prog. Polym. Sci.*, 2006, **31**, 603-632.

435 27. G. Crini, *Prog. Polym. Sci.*, 2005, **30**, 38-70.

436 28. L. Wang and A. Wang, *Bioresour. Technol.*, 2008, **99**, 1403-1408.

437 29. P. Wang and I. Lo, *Water Res.*, 2009, **43**, 3727-3734.

438 30. X. Guo, B. Du, Q. Wei, J. Yang, L. Hu, L. Yan and W. Xu, *J. Hazard. Mater.*,

439 2014, **278**, 211-220.

440 31. X. Yang, X. Zhang, Y. Ma, Y. Huang, Y. Wang and Y. Chen, *J. Mater. Chem.*,

441 2009, **19**, 2710-2714.

442 32. Y. Sun, Z.-l. Chen, X.-x. Yang, P. Huang, X.-p. Zhou and X.-x. Du,

443 *Nanotechnology*, 2009, **20**, 135102.

444 33. Z. Roveimiab, A. R. Mahdavian, E. Biazar and K. S. Heidari, *J. Colloid Sci.*

445 *Biotechnol.*, 2012, **1**, 82-88.

446 34. D.-S. Jiang, S.-Y. Long, J. Huang, H.-Y. Xiao and J.-Y. Zhou, *Biochem. Eng.*

447 *J.*, 2005, **25**, 15-23.

35. J. Zhu, P. C. Wang and M. Lu, *New J. Chem.*, 2012, **36**, 2587-2592.

36. L. Ma'mani, S. Miri, M. Mahdavi, S. Bahadorikhalili, E. Lotfi, A. Foroumadi and A. Shafiee, *RSC Adv.*, 2014, **4**, 48613-48620.

37. D. DelaiáSun, *New J. Chem.*, 2011, **35**, 137-140.

38. L. Li, H. Duan, X. Wang and C. Luo, *New J. Chem.*, 2014.

39. L. Fan, C. Luo, M. Sun, X. Li, F. Lu and H. Qiu, *Bioresour. Technol.*, 2012, **114**, 703-706.

40. L. Fan, C. Luo, X. Li, F. Lu, H. Qiu and M. Sun, *J. Hazard. Mater.*, 2012, **215**, 272-279.

41. D. C. Marcano, D. V. Kosynkin, J. M. Berlin, A. Sinitskii, Z. Sun, A. Slesarev, L. B. Alemany, W. Lu and J. M. Tour, *ACS nano*, 2010, **4**, 4806-4814.

42. P. P. Selvam, S. Preethi, P. Basakaralingam, N. Thinakaran, A. Sivasamy and S. Sivanesan, *J. Hazard. Mater.*, 2008, **155**, 39-44.

43. C. Moreno-Castilla, M. Alvarez-Merino, M. López-Ramón and J. Rivera-Utrilla, *Langmuir*, 2004, **20**, 8142-8148.

44. Y. Gao, Y. Li, L. Zhang, H. Huang, J. Hu, S. M. Shah and X. Su, *J. Colloid. Interface. Sci.*, 2012, **368**, 540-546.

45. W. Song, X. Wang, Q. Wang, D. Shao and X. Wang, *Phys. Chem. Chem. Phys.*, 2015, **17**, 398-406.

46. Y. Zhang, L. Yan, W. Xu, X. Guo, L. Cui, L. Gao, Q. Wei and B. Du, *J. Mol. Liq.*, 2014, **191**, 177-182.

47. X. Xin, Q. Wei, J. Yang, L. Yan, R. Feng, G. Chen, B. Du and H. Li, *Chem.*

Eng. J., 2012, **184**, 132-140.

48. Z. Jia, Q. Wang, D. Ren and R. Zhu, *Appl. Surf. Sci.*, 2013, **264**, 255-260.

49. S. Erentürk and E. Malkoç, *Appl. Surf. Sci.*, 2007, **253**, 4727-4733.

50. G. Xie, P. Xi, H. Liu, F. Chen, L. Huang, Y. Shi, F. Hou, Z. Zeng, C. Shao and J. Wang, *J. Mater. Chem.*, 2012, **22**, 1033-1039.

51. A. Debrassi, A. F. Corrêa, T. Baccarin, N. Nedelko, A. Ślawska-Waniewska, K. Sobczak, P. Dłużewski, J.-M. Greneche and C. A. Rodrigues, *Chem. Eng. J.*, 2012, **183**, 284-293.

52. J. Zhang, B. Li, W. Yang and J. Liu, *Ind. Eng. Chem. Res.*, 2014, **53**, 10629-10636.

53. M. Namvari and H. Namazi, *Polym. Int.*, 2014, **63**, 1881-1888.

54. L. Ai, H. Huang, Z. Chen, X. Wei and J. Jiang, *Chem. Eng. J.*, 2010, **156**, 243-249.

55. H. Sun, L. Cao and L. Lu, *Nano Res.*, 2011, **4**, 550-562.

56. A. Mohammadi, H. Daemi and M. Barikani, *Int. J. Biol. Macromol.*, 2014, **69**, 447-455.

57. Ö. Kerkez and Ş. S. Bayazit, *J. Nanopart. Res.*, 2014, **16**, 1-11.

58. L. Cui, X. Guo, Q. Wei, Y. Wang, L. Gao, L. Yan, T. Yan and B. Du, *J. Colloid. Interface. Sci.*, 2015, **439**, 112-120.

59. M. R. Unnithan and T. Anirudhan, *Ind. Eng. Chem. Res.*, 2001, **40**, 2693-2701.